LOSS GENERATION IN RADIAL OUTFLOW STEAM TURBINE CASCADES

A. Grönman - A. Uusitalo - J. Backman

Larjola Laboratory of Turbomachinery, Lappeenranta University of Technology, Lappeenranta, Finland, gronman@lut.fi

ABSTRACT

Small high-speed technology based radial outflow steam turbines are characterised by ultra-low aspect ratios, which can lead to rapidly growing secondary losses. The preliminary evaluation of turbine performance is usually based on axial turbine loss predictions, which can be a source of error. The main objectives of this work are to find out how the losses are generated in radial outflow turbines when the aspect ratio is markedly below unity and how accurately axial turbine loss models can predict the trends. To achieve these objectives, a radial outflow turbine cascade having a blade shape and aspect ratios comparable with a prototype machine is examined. As a result of the study, it is suggested that for the examined radial outflow cascade the axial turbine loss correlations can predict the trends reasonably well. The rapidly increasing secondary losses are connected to the merging of secondary structures and also incidence at off-design.

KEYWORDS

RADIAL OUTFLOW TURBINE, LOSSES, INCIDENCE

NOMENCLATURE

Latin alphabet

C	chord length	[m]
CR	convergence ratio, $cos(\alpha_1)/cos(\alpha_2)$	[-]
F_t	tangential loading parameter	[-]
h	blade height	[m]
p	static pressure	[Pa]
p_t	total pressure	[Pa]
R	gas constant	[J/kgK]
r	grid refinement factor	[-]
s	blade pitch	[m]
Y	loss coefficient	[-]
y^+	non-dimensional wall distance	[-]
Z_{te}	separation line height	[m]
AR	aspect ratio, h/c	[-]

Greek alphabet

α	absolute flow angle from radial direction	[°]
δ^*	boundary layer displacement thickness	[m]
Γ	stagger angle from radial direction	[°]
γ	ratio of specific heat constants	[-]
ω	total pressure loss coefficient, $1 - p_{t2}/p_{t1}$	[-]

Abbreviations

ORC	organic Rankine cycle
ROT	radial outflow turbine

Subscripts

1	cascade inlet
2	cascade outlet
ave	average
m	mean
mid	midspan
prim	primary
sec	secondary
x	axial

INTRODUCTION

In the utilisation of waste heat, different methods have been used depending on the size of the turbine and the temperature of the heat source. Typically, below 2 MWe an Organic Rankine Cycle (ORC) is used to recover the available energy. There are, however, several places where the use of a conventional Rankine cycle would be feasible instead of adding a closed loop ORC power plant with an additional heat exchanger. Such applications include e.g. biomass power plants during low loads, saw mills, and large ships. All of the mentioned applications can offer waste steam which can be utilised by adding a hermetic turbogenerator (Leino et al. 2016) to produce electricity directly from the waste heat steam stream. The design presented by Leino et al. (2016) is composed of a hermetic, water-cooled electric machine using magnetic bearings and a radial outflow turbine (ROT). The designed four-stage turbine is characterised by ultra low aspect ratios (AR) and also by large relative tip clearances.

A very limited number of public-access studies are available about radial outflow turbine design and fluid dynamics. Recently, this turbine type has been studied for ORC applications e.g. (Pini et al. 2013, Persico et al. 2013, Casati et al. 2014), and in the 1970s, for solar Rankine applications (Martin & Kolenc 1979).

Pini et al. (2013) coupled 1D mean-line code with a genetic algorithm and throughflow solver to design a 1000 kW ROT-ORC. Later, Casati et al. (2014) performed a study for a mini ORC system that employed radial outflow turbines. Their design procedure also coupled a meanline design tool and genetic algorithm.

Persico et al. (2013) examined different blade shapes in both axial and radial outlow configurations. The axial turbine blades were transferred to a conical plane by conformal mapping. The study indicated that front-loaded converging blade channels in axial configuration generate converging-diverging channels in ROT cascades, and improved performance can be achieved by more regular curvature and loading distribution. The study also concluded that classical axial turbine profile loss correlations over-predict slightly centrifugal cascade losses. This behaviour was connected to the lower growth of rear suction side boundary layer and thus, weaker wakes in radial outflow cascades compared to axial designs.

Persico et al. (2015) studied both stator and rotor cascades by including also the rotational effects into their model. The effects of the centrifugal force and diverging shape of the blade channel were found to cause significant changes to the pressure distribution of the rotor blade. The study also provided a detailed analysis of the secondary flow field after the stator which was characterised by strong secondary vortex behaviour.

The effect of the ultra-low aspect ratio ($h/c < 1$) is also studied very limitedly in the literature. Kuno and Sonoda (2004) suggest that the primary cause of the poor performance with the ultra-low AR is the increase of secondary losses. They maintain that the predictions of axial turbine loss correlations, such as those by Kacker and Okapuu (1981), cannot be verified at an AR below unity. This leaves room for speculation whether the secondary losses increase as rapidly as the prediction suggests. If the secondary losses do not develop as predicted, the use of an ultra-low AR may be more feasible than expected.

At some ultra-low AR value, the passage vortices can meet at the midspan. A similar assumption was also made by Benner et al. (2006*a*), as they developed their penetration depth correlation, which can be used to evaluate the AR which allows the passage vortex separation lines to meet at the midspan. Sonoda et al. (2008) have presented both an experimental and a numerical analysis on the flow mechanisms of an annular ultra-low AR inlet guide vane. Their flow visualisations gave indications that the typical separation lines do not exist at AR=0.21.

From the existing information, the current study continues the already ongoing evaluation of the suitability of axial turbine loss correlations on the radial outflow turbine performance prediction by evaluating the accuracy of relatively recent methods. Special attention is also paid to the loss source analysis of ultra-low AR blades. First, the modelling methods are described, and second, they are followed by a presentation of the examined blade geometry. Third, the results of the grid dependency study are presented. Finally, the effects of the AR and incidence are studied and compared with axial turbine loss correlations.

METHODS

Numerical methods

The Navier-Stokes solver Finflo is used in this study. The solver has been succesfully used to model both linear (Grönman et al. 2013) and centrifugal turbine cascades (Harinck et al. 2010). It employs the finite-volume method for spatial discretisation and uses a constant specific heat capacity at constant pressure. More detailed information about Finflo and different numerical methods can be found e.g. in a paper by Siikonen (1995).

In this study, a k-ω-SST turbulence model (Menter 1993) without wall functions has been used, and the fluid is modelled as an ideal gas with R=462.5 J/kgK and γ=1.32. This assumption is reasonable since the compressibility factor of dry steam at relatively low operational pressure and temperature levels is close to unity during the whole expansion.

Uniform momentum and total enthalpy distributions are defined as the inlet boundary conditions, and a constant static pressure distribution is used as the boundary condition at the outlet. Where applicable, cyclic boundaries are employed. The boundary conditions are presented in Fig. 1 (a). Additionally, the hub and shroud walls are modelled as solid walls in three-dimensional models, and in two-dimensional models, symmetry boundary condition is used. In post-processing the values at the inlet are calculated slightly downstream from the inlet boundary (plane 1), and at the outlet, slightly upstream from the outlet boundary at 48% of the radial chord (plane 2) downstream from the trailing edge to ensure fully mixed out conditions. The values at the circumferential measurement planes 1 and 2 are mass flow averaged.

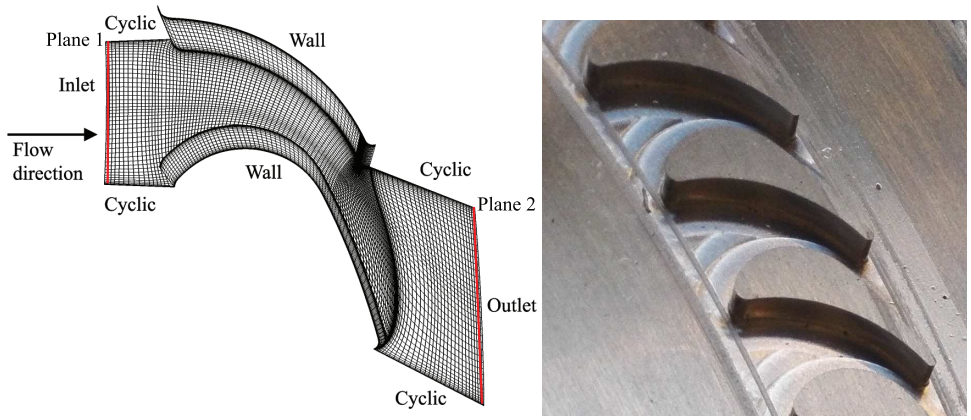

Figure 1: **Example of the modelled geometry with h/c=0.26 (a) and the real turbine rotor geometry after test milling (b).**

During the simulations, the convergence is monitored by following the mass flow difference

between the inlet and outlet, and the mass flow is considered to be converged when the difference is stabilised. In addition, the L2 norms of density, momentum in all three directions, and energy residuals are important convergence parameters.

Loss evaluation methods

The losses in CFD simulations are divided into primary and secondary losses where the total mixed out losses are defined as the sum of primary and secondary losses

$$Y_{total} = Y_{prim} + Y_{sec}, \tag{1}$$

where the total mixed out losses are defined as

$$Y_{total} = \frac{p_{t1} - p_{t2}}{p_{t2} - p_2}. \tag{2}$$

In Equation 1, the primary losses are calculated with the penetration depth correlation of Benner et al. (2006*a*) to include the effect of passage vortex separation lines on the primary loss as follows:

$$Y_{prim} = Y_{mid}(1 - \frac{Z_{te}}{h}). \tag{3}$$

Where Z_{te} is the separation line height and is defined as the height of the secondary region at the blade trailing edge and Y_{mid} is the total mixed out loss from two dimensional CFD. Benner et al. (2006*a*) states that the maximum realizable value of Z_{te}/h=0.5 occurs when the passage vortex separation lines from each end-wall meet at midspan. As is later shown in Fig. 3 (b) the maximum realizable value is reached at the lowest aspect ratio or even earlier as predicted by CFD. To keep the cases in Fig. 3 (a) comparable to each other the penetration depth correlation is applied even if the maximum value is exceeded. However, at the off-design incidence it is assumed that the maximum realizable value has been exceeded and $Y_{prim} = Y_{mid}$. The penetration depth Z_{te}/h is defined as

$$\frac{Z_{te}}{h} = \frac{0.1F_t^{0.79}}{\sqrt{C\bar{R}}(h/C)^{0.55}} + 32.70(\frac{\delta^*}{h})^2. \tag{4}$$

Where the tangential loading parameter F_t is defined as

$$F_t = 2\frac{s}{C_x}cos^2\alpha_m(tan\alpha_1 - tan\alpha_2), \tag{5}$$

and the mean mean vector angle α_m may be solved from

$$tan\alpha_m = \frac{1}{2}(tan\alpha_1 + tan\alpha_2). \tag{6}$$

In the one-dimensional loss calculations, the Y_{mid} is evaluated based on the prediction method by Kacker and Okapuu (1981), and the secondary loss correlation of Benner et al. (2006*b*) is used to predict the secondary losses in blade cascade as follows

$$Y_{sec} = \frac{0.038 + 0.41tanh(1.20\delta^*/h)}{\sqrt{cos\Gamma}(CR)(h/C)^{0.55}(\frac{Ccos\alpha_2}{C_x})^{0.55}}. \quad (7)$$

For the calculation of one-dimensional off-design primary losses, the correlation of Benner et al. (1997) is employed relative to the primary losses from CFD simulations at zero incidence.

BLADE GEOMETRY AND STUDIED CASES

The examined geometry is a non-scaled model of the first-stage rotor (Fig. 1 (b)) used in a four-stage turbine protype. Table 1 shows the main design parameters of the blade cascade. The basic design is characterised by an ultra-low aspect ratio and relatively low Mach number. Overall, five aspect ratios were studied, in the range $0.26 \leq h/c \leq 1.58$. When the aspect ratio was varied, the number of spanwise cells was kept comparable between different cases. This means that e.g. when the aspect ratio and also the blade height was doubled the number of spanwise cells was doubled as well and the same node distribution function was used for both cases. The Reynolds number and Mach number were also kept constant between the modelled cases to keep the simulations comparable. Although it is known from the work of Persico et al. (2015) that the rotation of the rotor can greatly influence the flow in a ROT, this work is closely connected to stationary cascade experiments and the capability of axial turbine loss models to predict the performance in an early design phase, and the influence of rotation is therefore not included in this work.

Table 1: **Blade cascade design parameters.**

Aspect ratio [-]	0.26	Blade inlet Mach number [-]	0.23
Pitch to chord ratio [-]	0.71	Blade outlet Mach number [-]	0.40
Reynolds number [-]	575000	Blade inlet metal angle [°]	47.5
Total-to-static pressure ratio [-]	1.15	Blade outlet flow angle [°]	-67.3

GRID DEPENDENCY

A total of six grids (three grids for both 2D and 3D) were built to examine how the grid affects the results. The case with the lowest aspect ratio $h/c = 0.26$ was used in the study. The grid convergence index method by Celik et al. (2008) was used to evaluate the discretisation error. As shown in Table 2, the average non-dimensional wall distance y^+ was kept below unity at every 2D grid and slightly higher, but still acceptable, values are noticed when changing to 3D geometries. Since the height of the first cell is constant between all two and three dimensional cases, the slightly higher y^+ values are due to three dimensional effects. The grid refinement factor r is suggested to be greater than 1.3 by Celik et al. (2008). All 2D grids satisfy this value, and the 3D grids are just below the limit. This is still acceptable, since the general idea was to first find a reasonably grid-independent 2D grid, which was then modified to 3D by only changing the number of spanwise cells by doubling the cell number.

Figure 2 (a) shows the effect of the grid on the total mixed out loss coefficient in 2D. It is noticeable that by almost doubling the number of cells from the medium grid, the loss coefficient does not change significantly. Also, the isentropic Mach number distribution in Fig. 2 (c)

Table 2: **Grids used in the grid dependency study. Number of cells are presented in pitch-wise, radial and spanwise directions, respectively.**

Type	Cells	$y^+_{ave,max}$	r	Type	Cells	$y^+_{ave,max}$	r
2D	33x77x1	0.6	1.4	3D	48x124x8	3.4	1.3
2D	48x112x1	0.6	1.5	3D	48x124x16	3.4	1.3
2D	66x176x1	0.6	-	3D	48x124x32	3.7	-

remains very similar between the two grids. This leads to the conclusion that the medium grid gives reasonably grid-independent results and it is chosen to be the basis for the 3D grid generation. Figure 2 (b) shows that the number of spanwise cells has a small influence on the total pressure loss coefficient. Although not shown here, the isentropic Mach number distribution at the midspan is slightly less affected by the grid modification than with the 2D grids. As a result, the most dense grid was chosen to be the basis for simulations with different aspect ratios, even though, the medium 3D grid could also provide acceptable results.

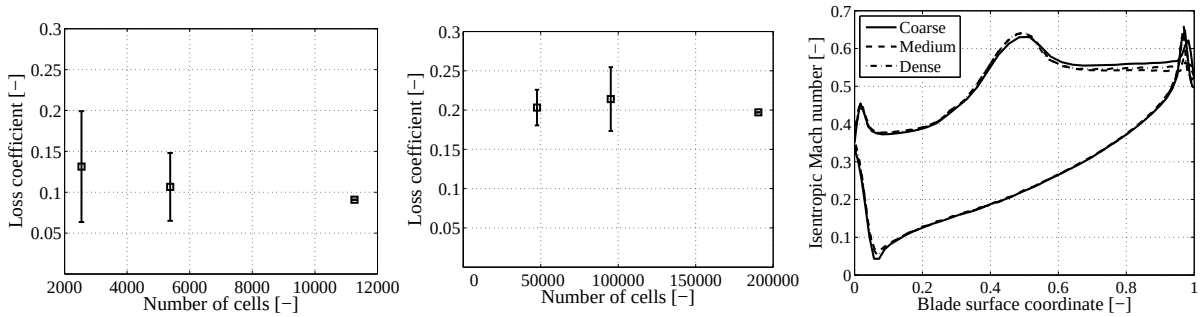

(a) (b) (c)

Figure 2: **Effect of grid density on total mixed out loss coefficient and discretisation error in 2D grids (a), 3D grids (b) and (c) on 2D isentropic Mach number distribution.**

RESULTS

Loss Generation With Different Aspect Ratios

The influence of the aspect ratio on the predicted primary and secondary losses is presented in Fig. 3 (a). Overall, the trends of primary losses have similar shapes and show a slightly decreasing trend with a decreasing aspect ratio. In the area of ultra-low aspect ratios $h/c < 1$, the primary losses are predicted to have a gradually decreasing trend by both models, whereas the secondary losses exhibit the opposite trend. Overall, both models support the previous understanding that the secondary losses are responsible for the rapid loss increase in ultra-low aspect ratio turbines. The secondary loss trend predicted by the CFD simulations at ultra low aspect ratios is slightly steeper than the 1D model predicts, however, more geometries should be studied to be able to generalise.

The main reason for the observed differences between primary loss predictions is that the 1D model does not include trailing edge losses as part of the primary losses, as the CFD model

does. This loss is estimated according to the model by Kacker and Okapuu (1981) and leads to slight over prediction compared to the CFD model. The finding is also in line with that of Persico et al. (2013), who found that the classical axial turbine profile loss models slightly overpredict losses in comparison with the numerical results in transonic turbine cascade. To make a general conclusion from the loss overprediction, more data should be available with different loss models and Mach numbers.

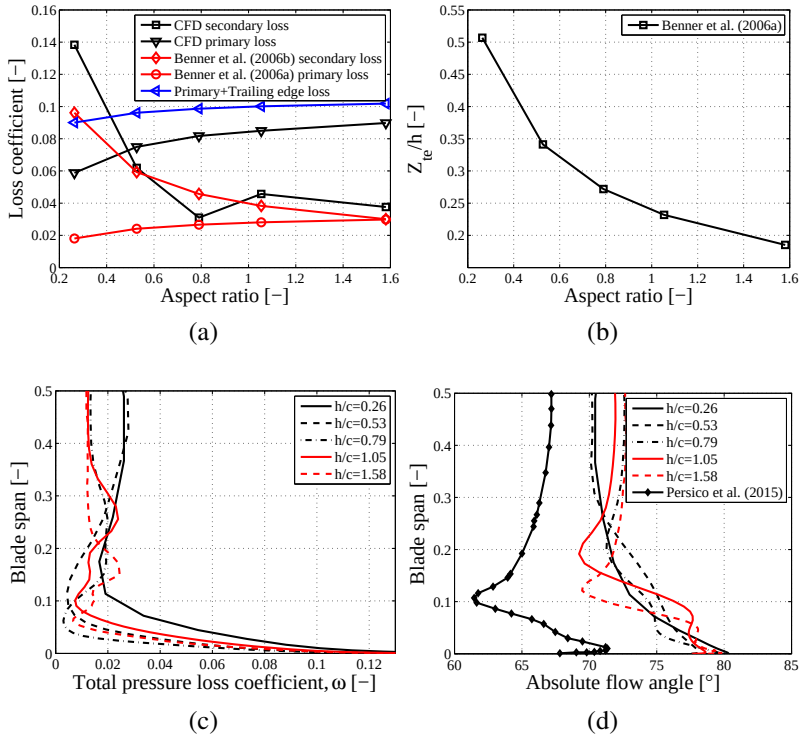

Figure 3: **The effect of the aspect ratio on primary and secondary losses (a), the predicted penetration depth as a function of the aspect ratio (b), the effect of the aspect ratio on the spanwise total loss profile (c) and absolute flow angle (d).**

In the prediction of the passage vortex separation line, Eq. 4 predicts that the passage vortices should meet with the smallest studied aspect ratio at the trailing edge as shown in Fig. 3 (b). This means that the use of penetration depth correlation in Eq. 3 is justified also at the smallest aspect ratio in Fig. 3 (a), which makes the comparison between the cases also straight forward. In comparison, the numerical simulations predict that the secondary vortices merge before the trailing edge with AR=0.26, but also with AR=0.53 the vortices have merged. This merging behaviour is noticeable both in spanwise total pressure loss profiles in Fig. 3 (c) and in contour plots of Figs. 4 (a) and (b). In spanwise loss profiles the vortex merging also explains why the midspan losses in Fig. 3 (c) are clearly higher for the lowest two aspect ratios and also why the absolute flow angles for the same cases separate from others in Fig. 3 (d). When the AR is 0.79, two loss cores surrounded by separate vorticity peaks are visible in Figs. 4 (c) and (d), suggesting that two separate and relatively weak loss cores still exist.

The influence of secondary flows on turning the flow angle is visible in Fig. 3 (d), which compares the current results with the ROT stator from Persico et al. (2015). The areas of over-

turning due to end-wall cross-flow and the underturning due to secondary vortices are present with the $h/c = 1.58$ and also still with $h/c = 0.79$. However, when the secondary structures begin to merge, the typical spanwise flow angle distribution no longer shows the underturning, although the effect of cross-flow is still visible. The mixing of hub and shroud side secondary structures is also predicted to lead to a more uniform flow angle distribution, which can be beneficial for the downstream blade row even though the losses after the stator are higher.

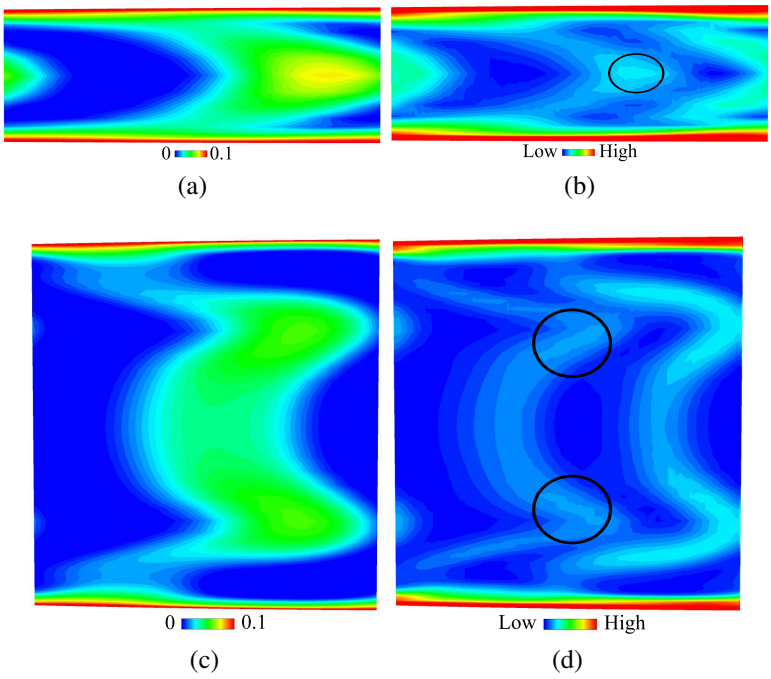

Figure 4: **Contours of the total pressure loss coefficient (left) and vorticity magnitude (right) at the cascade outlet (plane 2) with AR=0.26 (a-b) and AR=0.79 (c-d).**

Influence of Incidence

The effect of incidence on the development of primary and secondary losses is presented in Fig. 5 (a). The basic design with AR=0.26 is used in these simulations, and in the calculation of primary losses it is assumed that Y_{prim}=Y_{mid} with all incidences. This assumption also explains why the losses in Fig. 3 (a) differ from Fig. 5 (a). A small CFD underprediction of primary loss change is found with negative incidence and overprediction at positive incidence, predicting a greater increase in losses at positive incidence. In comparison, a slight underprediction was found by Persico et al. (2013) when comparing their 2D CFD with the prediction of the method by Craig and Cox (1971) for incidence changes of $\pm$20 degrees. The secondary losses are predicted to increase with incidence and are connected to stronger vorticity, as shown in Figs. 6 (c) and (d).

The influence of incidence is clearly visible in the front part of the blade in Fig. 5 (b), as presented also by Persico et al. (2013). A negative incidence leads to lower loading on the first 30 per cent of the blade surface mainly due to changes on the suction side, whereas a positive incidence increases loading. When the effect of 3D phenomena is evaluated at the midspan in Fig. 5 (c), it can be seen that these effects do not have a great influence on the front part of the

blade due to separate hub and shroud secondary structures, but especially the last 40 per cent of the blade surface on the suction side is clearly affected, although the influence of incidence is practically negligible. These changes in loading are further connected to the merging of secondary structures at the midspan.

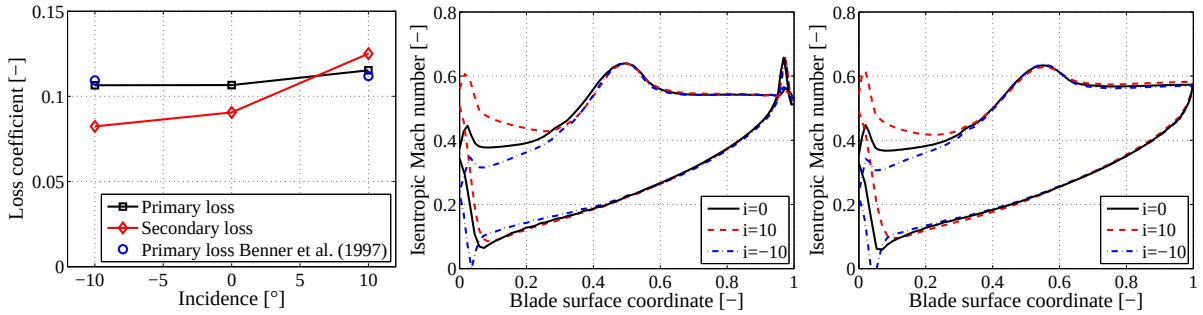

Figure 5: **The effect of incidence on primary and secondary losses (a) and the isentropic Mach number distribution on 2D (b) and 3D geometries (c).**

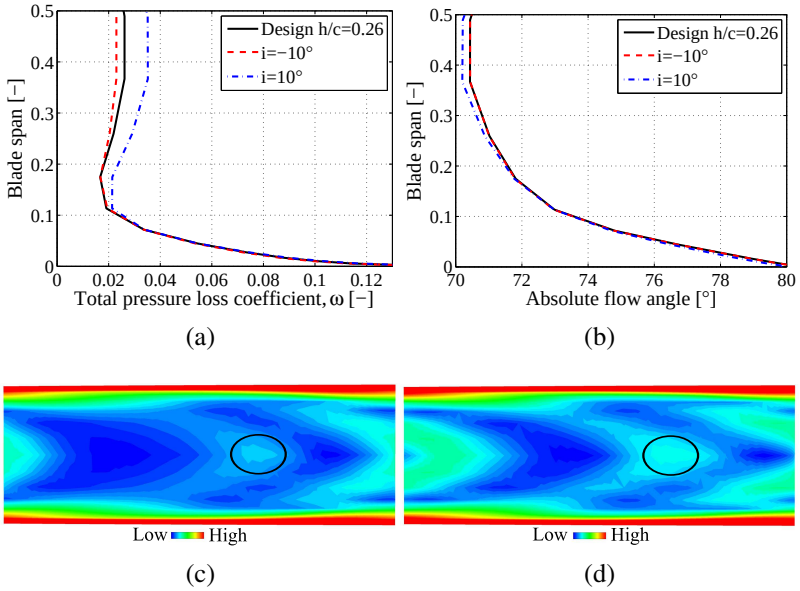

Figure 6: **The effect of incidence on the spanwise total pressure loss coefficient (a), absolute flow angle (b), and contours of vorticity at negative (c) and positive incidence (d) in plane 2.**

The influence of positive incidence on spanwise total pressure loss is reasonably high above 10% of the span in Fig. 6 (a). There is a noticeable change in the position and strength of the vorticity (and total pressure loss) in the mentioned area, as shown in Figs. 6 (c) and (d), and it was linked to increasing secondary losses. However, only a minor effect is seen in Fig. 6

(b) on the absolute flow angle distribution, which can be considered positive for the following stator/rotor blade in a real turbine and supports the expected good off-design behaviour of the ROT.

CONCLUSIONS

This study suggests that for the examined radial outflow blade cascade, the secondary losses exhibit a similar rapidly increasing trend as the one-dimensional axial turbine secondary loss prediction method predicts at an ultra-low aspect ratio region with a steeper increase. The passage vortex merging at the trailing edge is predicted numerically to occur at slightly higher aspect ratios than the one-dimensional method predicts. The noticed secondary structure merging process leads to an excessive increase in secondary losses and is also responsible for the increase in total mixed out losses. When including the trailing edge losses in both models, the CFD simulations underpredict the losses compared to the axial turbine loss correlation, which qualitatively supports the previous results.

In off-design conditions, the position of secondary structures was affected together with the associated loss cores. The change in the vorticity magnitude was also realised as increased secondary losses. However, the absolute flow angle after the blade was only slightly affected by the change of incidence. This finding supports the expected good off-design behaviour of the radial outflow turbine. Overall, the primary losses were slightly under or over predicted by the numerical ROT model compared to the axial turbine off-design loss correlation.

In the future, more research should be conducted to understand the secondary structures' merging process better. In addition, the current results should be experimentally verified in the future. Also the possibility to expand the stationary results into rotational frame from should be examined more.

ACKNOWLEDGEMENTS

This work has been carried out in the framework of Herge project funded by Tekes - the Finnish Funding Agency for Innovation and the radial outflow cascade test rig investment project funded by Lappeenranta University Technology.

REFERENCES

Benner, M. W., Sjolander, S. A. & Moustapha, S. H. (1997), 'Influence of Leading-Edge Geometry on Profile Losses in Turbines at Off-Design Incidence: Experimental Results and an Improved Correlation', *Journal of Turbomachinery* **119**, 193–200.

Benner, M. W., Sjolander, S. A. & Moustapha, S. H. (2006*a*), 'An Empirical Prediction Method for Secondary Losses in Turbines-Part I: A New Loss Breakdown Scheme and Penetration Depth Correlation', *Journal of Turbomachinery* **128**, 273–280.

Benner, M. W., Sjolander, S. A. & Moustapha, S. H. (2006*b*), 'An Empirical Prediction Method for Secondary Losses in Turbines-Part II: A New Secondary Loss Correlation', *Journal of Turbomachinery* **128**, 281–291.

Casati, E., Vitale, S., Pini, M., Persico, G. & Colonna, P. (2014), 'Centrifugal Turbines for Mini-Organic Rankine Cycle Power Systems', *Journal of Engineering for Gas Turbines and Power* **136**, 122607.

Celik, I., Ghia, U., Roache, P., Freitas, C., Coleman, H. & Raad, P. (2008), 'Procedure for Estimation and Reporting of Uncertainty Due to Discretization in CFD Applications', *Journal of Fluids Engineering* **130**, 078001.

Craig, H. R. M. & Cox, H. J. A. (1971), 'Performance Estimation of Axial Flow Turbines', *Proceedings of the Institution of Mechanical Engineers* **185**, 407–424.

Grönman, A., Turunen-Saaresti, T., Röyttä, P., Jaatinen, A. & Backman, J. (2013), 'Performance and Flow Fields of a Supersonic Axial Turbine at Off-Design Conditions', *Proceedings of the Institution of Mechanical Engineers, Part A: Journal of Power and Energy* **227**, 285–294.

Harinck, J., Turunen-Saaresti, T., Colonna, P., Rebay, S. & van Buijtenen, J. (2010), 'Computational Study of a High Expansion Ratio Radial Organic Rankine Cycle Turbine Stator', *Journal of Engineering for Gas Turbines and Power* **132**, 054501.

Kacker, S. C. & Okapuu, U. (1981), 'A Mean Line Prediction Method for Axial Flow Turbine Efficiency', *Journal of Engineering for Power* **104**, 111–119.

Kuno, N. & Sonoda, T. (2004), 'Flow Characteristics in a Transonic Ultra-Low-Aspect-Ratio Axial Turbine Vane', *Journal of Propulsion and Power* **20**, 596–603.

Leino, M., Uusitalo, V., Grönman, A., Nerg, J., Horttanainen, M., Soukka, R. & Pyrhönen, J. (2016), 'Economics and Greenhouse Gas Balance of Distributed Electricity Production at Sawmills Using Hermetic Turbogenerator', *Renewable Energy* **88**, 102–111.

Martin, C. & Kolenc, T. (1979), Study of Advanced Radial Outflow Turbine for Solar Steam Rankine Engines, Technical Report NASA-CR-159695.

Menter, F. R. (1993), Zonal Two Equation $k - \omega$ Turbulence Models for Aerodynamic Flows, *in* '24th AIAA Fluid Dynamics Conference, Orlando, Florida, AIAA Paper 93-2906'.

Persico, G., Pini, M., Dossena, V. & Gaetani, P. (2015), 'Aerodynamics of Centrifugal Turbine Cascades', *Journal of Engineering for Gas Turbines and Power* **135**, 042312.

Persico, G., Pini, P., Dossena, V. & Gaetani, P. (2013), Aerodynamic Design and Analysis of Centrifugal Turbine Cascades, *in* 'Proceedings of ASME Turbo Expo, June 3-7, 2013, San Antonio, Texas, USA', number GT2013-95770.

Pini, M., Persico, G., Casati, E. & Dossena, V. (2013), 'Preliminary Design of a Centrifugal Turbine for Organic Rankine Cycle Applications', *Journal of Engineering for Gas Turbines and Power* **135**, 042312.

Siikonen, T. (1995), 'An Application of Roe's Flux-Difference Splitting for the $k-\epsilon$ turbulence model', *International Journal for Numerical Methods in Fluids* **21**, 1017–1039.

Sonoda, T., H. M. A. T. & Sendhoff, B. (2008), 'Effect of Endwall Contouring on Performance of Ultra-Low Aspect Ratio Transonic Turbine Inlet Guide Vanes', *Journal of Turbomachinery* **131**, 011020.